ANALYSIS OF MAN-MADE TARGET DETECTION IN SAR IMAGERY

Wang Changlin, Zhong Xuelian

Institute of Remote Sensing Applications, Chinese Academy of Sciences

P.O. Box 9718, No.3 Datun Rd., Chaoyang District Beijing 100101, China

Tel: 86-10-64838047 Fax: 86-10-64879740

Email: wcl@irsa.ac.cn

ABSTRACT

Automatic target detection in SAR image is the first stage in the ATR (Automatic Target Recognition) system. It is very important to improve the computing efficiency of the whole system. A conventional automatic target detection method is CFAR (constant false alarm rate) which is based only on the amplitude, discards the phase and thereby sacrifices half information of the SAR imagery. Almost each CFAR brings a large number of false alarms. 2L-IHP (two-look internal Hermitian product) is a new method which exploits the phase and amplitude information. In this paper, both CFAR and 2L-IHP algotithms are compared with an emphasis on 2L-IHP. The 2L-IHP algorithm for target detection is discussed briefly first. In order to apply it widely, it is modified to circumvent the constraint of the data. For polarimetric SAR images, PWF (Polarimetric Whitening Filter) is used to generate an image for target detection. According to ADTS data set, these algorithms are analyzed and evaluated respectively. C-、L- and P- band AIRSAR data are also processed, and some tentative conclusions are derived: Considering the penetrating ability of the microwave, L-band got the best detection accuracy of the three bands; HH polarization performed better for target detection than VV and HV polarization; Moreover, because more information is contained in polarimetric SAR data, here, we conclude that polarimetric SAR data have advantages over single polarized SAR data when they are applied for target detection. But all these conclusions need further validation.

1. INTRODUCTION

Automatic target detection and recognition are important for civil and military applications, such as detecting the underground pipes, inspecting the tanks in the trees and ships on the sea, searching and rescuing the crashed aircraft, etc. Because Synthetic Aperture Radar (SAR) has the two primary advantages: all–weather and day or night imaging, target detection and recognition in SAR imagery will have wider applications in the present and the future. Due to the large difference between the stationary target detection and mobile target detection in SAR imagery, we focus our attention to detect the stationary targets in SAR imagery.

A typical automatic target recognition system consists of three stages: detection, discrimination and classification (Figure1). The detection stage is to find regions in SAR imagery that contain potential targets. The algorithms in this part should be as simple as possible because of the huge computation cost here. The probability of detection in this stage had better be close to 100%, but the probability of false alarm will increase greatly with the probability of detection. These false alarms can be further reduced by the following stage: discrimination. The two stages together are called prescreening. Classification is to determine which class the target belongs to. The prescreening component is very important in the whole ATR system. If it acts high effectively, that is to say, it can reject almost all the background clutter, the computational cost in the process of classification will be greatly reduced.

Figure 1: Flowchart for ATR system

A lot of algorithms have been developed to detect targets in SAR imagery. CFAR algorithms (Constant False Alarm Rate) have been applied widely among them. However, CFAR and its improved algorithms have to build a statistical model for the clutter. Since there are a number of factors influencing the clutter, for example, the type of the ground, it is difficult to build an accurate model to simulate the clutter. When the targets are adjacent to each other, CFAR algorithms can not work. 2L-IHP (Two-Look Internal Hermitian Product) overcomes these two disadvantages and produces better detecting results than traditional CFAR algorithms. This paper compares the two algorithms and analyzes 2L-IHP emphatically. The paper is organized as follows: Section 2 talks about the target detecting algorithms, including CFAR and 2L-IHP; Section 3 compares CFAR and 2L-IHP; Adjustment and improvement of 2L-IHP algorithm are discussed in Section 4 to circumvent the data constraint; the last section concludes the paper.

Proc. 'Envisat Symposium 2007', Montreux, Switzerland
23–27 April 2007 (ESA SP-636, July 2007)

2. ALGORITHMS

2.1 CFAR

Common CFAR algorithms include: CA-CFAR (Cell-Averaging) (Koch and Moya, 1995), Two-parameter CFAR (Burl et al., 1989), SEG-CFAR (Segmentation-based CFAR) (McConnell and Olive, 1998 and 1999), Gamma CFAR (Principe and Radisavljevic, 1998), ML-CFAR (Maximum Likelihood CFAR) (Ravid and Levanon, 1992; Kuttikkad and Chellappa, 1994), etc. Two-parameter CFAR supposes that the clutter obeys the Gaussian distribution, and it compares the tested pixel to the mean and variance of the clutter. If the value exceeds a pre-defined threshold, the tested pixel will be marked as target pixel,

$$\frac{X_t - \overline{X_c}}{\sigma_c} \geq T_{CFAR} \quad (1)$$

Where X_t is the tested pixel, $\overline{X}_c$ and σ_c are the mean and variance of the clutter. Figure 2 is the stencil to compute the mean and variance of the background clutter. There is a warning area between the tested pixel and the clutter in order to reduce the influence of

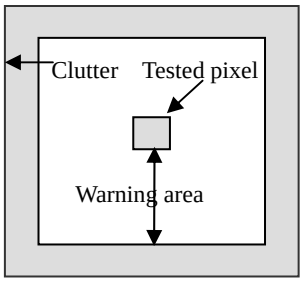

Figure.2: Top view of CFAR stencil

the targets. ML-CFAR is developed from two-parameter CFAR and applies the same stencil. The difference lies in that ML-CFAR considers the clutter obeys the Weibull or Rayleigh distribution with the parameters unknown, and the parameters are obtained by the maximum likelihood estimation. The PDF (Probability Density Function) of Weibull distribution is

$$p(x) = \begin{cases} \frac{C}{B}\left(\frac{x}{B}\right)^{C-1} \exp\left\{-\left(\frac{x}{B}\right)^{C}\right\}; & x \geq 0 \\ 0 & x < 0 \end{cases} \quad (2)$$

Where B is the scale parameter and C is the shape parameter. The maximum likelihood estimates of B and C, $\hat{B}$ and $\hat{C}$, are obtained from the M background samples

$$\hat{x} = (x_1, x_2, \ldots, x_M)^T \quad (3)$$

by solving iteratively the equations

$$\frac{\sum_{m=1}^{M} x_m^{\hat{C}} \ln x_m}{\sum_{m=1}^{M} x_m^{\hat{C}}} - \frac{1}{M}\sum_{m=1}^{M} \ln x_m = \frac{1}{\hat{C}} \quad (4)$$

$$\hat{B} = \left(\frac{1}{M}\sum_{m=1}^{M} x_m^{\hat{C}}\right)^{1/\hat{C}} \quad (5)$$

$$P_{FA} = \exp\left[-\left(\frac{T}{\hat{B}}\right)^{\hat{C}}\right] \quad (6)$$

Where P_{FA} is the desired probability of false alarm. The tested pixel is considered as target if its value exceeds the threshold T. The ROIs (Region Of Interest) are gained after a clustering process is applied to all the so-called target pixels.

2.2 2L-IHP

2L-IHP comes from sub-aperture coherence detection which was motivated by interferometric SAR (IFSAR) processing. It is well documented that specular targets correlate over larger variations in angular misregistration than clutter regions which require subpixel registration to enable high correlation (Meth, 2002). So correlation can be used to discriminate targets and clutter. The image pair can be obtained from a single SAR image by sub-aperture decomposition. In order to capture both radiometric and phase behaviors of the targets, Souyris proposed internal Hermitian product $\rho_{herm} = \langle s_1 \cdot s_2^* \rangle$ to represent the interferometric coherence, where s_1 and s_2 are the complex values associated with the image pair S_1 and S_2 for a given pixel, and $\langle \cdot \rangle$ is a spatial averaging in the vicinity of this pixel. Detailed 2L-IHP algorithm was shown in (Souyris et al., 2003) and (Henry et al., 2003).

Sub-aperture SAR images are generally obtained by selecting a Doppler sub-spectrum from a raw data set acquired by the sensor and by processing the corresponding image using a synthesis algorithm. But raw data are seldom distributed by the organizations in charge of SAR data collection. Fortunately, an equivalent result can be obtained by sampling a Doppler sub-spectrum within an already processed SAR image. This technique decomposes synthesized images into azimuthal sub-spectra and requires the use of a deconvolution procedure in order to compensate the effects of weighting functions and antenna pattern. Sub-aperture images are then created using an inverse Fourier transform (Famil et al., 2002). Removing the weighting functions in the azimuth and range directions in the sub-aperture decomposition process will greatly improve the 2L-IHP performance. In some certain situations, the coherence after removing the weighting functions is about twice that without this processing, which makes target detection much easier.

3. COMPARISON BETWEEN CFAR AND 2L-IHP ALGORITHMS

In this section, we will compare the detecting results of CFAR and 2L-IHP. The data used in this experiment is HH polarization, single look complex (SLC) image, selected from ADTS dataset collected by the Lincoln Laboratory[1]. Figure 3 and 5 are the experimental images, respectively named m85p3f21hh and m78p1f23hh. The size is 512 (azimuth) × 2048 (slant range), and the resolution is 1foot×1foot. The man-made targets in the images are tanks, APCs (Armored Personnel Carrier), howitzers and corner reflectors. Figure 4 and 6 are their ground truth images.

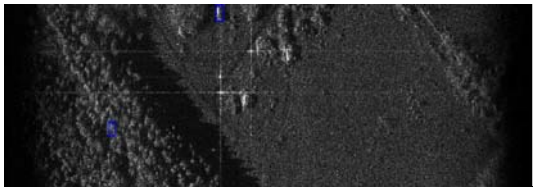

Figure3: Original SAR image of m85p3f21hh

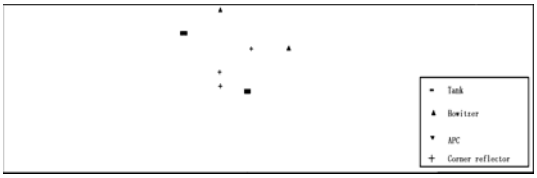

Figure 4: Ground truth image of targets in m85p3f21hh

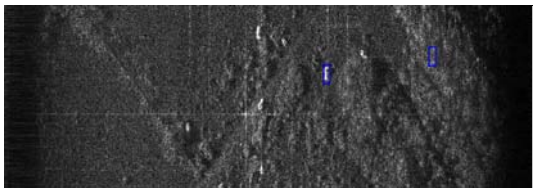

Figure 5: Original SAR image of m78p1f23hh

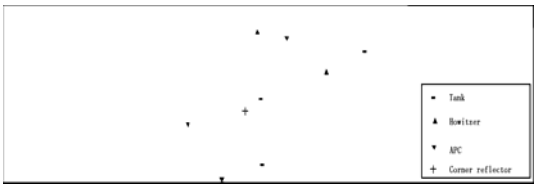

Figure 6: Ground truth image of targets in m78p1f23hh

In the ML-CFAR algorithm, the outer window of the stencil is 85×85，the inner window is 77×77，and the parameter B is equal to 2. Figure 7 is the detecting results of m85p3f21hh via ML-CFAR when the probability of false alarm equals 0.001. It is easily to see that a lot of non-target pixels trigger the threshold. Figure 8 shows the clustering results with the cluster window 15×15 and threshold 25%. All the 4 military targets are detected, but two corner reflectors are lost. Because the cluster window size is set according to the true size of the military targets, without considering the corner reflector size，ML-CFAR produces 7 false alarms.

Image m85p3f21hh and m78p1f23hh are processed via 2L-IHP, and their coherence images are displayed in Figure 9 and 10. All the man-made targets are detected no matter how small it is. It is easily to find that the results of m78p1f23hh look better than that of m85p3f21hh. This is because the military targets in the latter image are camouflaged and hidden, which weaken the backscattering signal greatly. When the coherence threshold is set to be 0.9, there are 2 false alarms in m85p3f21hh,

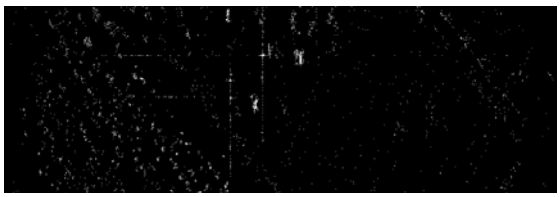

Figure 7: Detecting result of m85p3f21hh via ML-CFAR when P_{FA} = 0.001

Figure 8: Clustering image when clustering window is 15×15

and threshold is 25% (after dilation) and 2 false alarms in m78p1f23hh. From the detecting results of image m85p3f21hh, one can simply conclude that 2L-IHP algorithm is superior to CFAR method. In order to compare the two algorithms statistically, the whole public ADTS dataset are tested. Figure 11 shows the relationship between the probability of false alarm and the probability of detection for ML-CFAR and 2L-IHP. Figure 12 is the enlarged view of the low false alarm portion in Figure 11. Here, the probability of false alarm is defined as the number of false alarms per square kilometer. When the probability of detection is greater than 90%, large number of false alarms will be inevitably produced by ML-CFAR. However, 2L-IHP algorithm always achieves high probability of detection and low probability of false alarm. From the above experiments, it is apparent that 2L-IHP performs better than ML-CFAR in the probability of false alarm and the probability of detection. Moreover, 2L-IHP algorithm needn't construct the probability density function of the background clutter, and it is simple and easy to manipulate. All the factors mentioned above make

[1] Please consult the website https://www.sdms.afrl.af.mil/datasets/adts/.

2L-IHP algorithm superior to ML-CFAR algorithm.

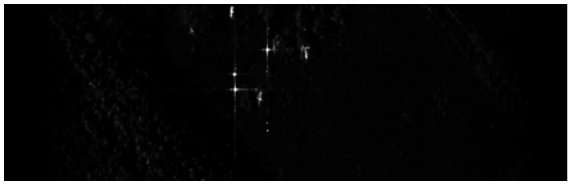

Figure 9: Coherence image of m85p3f21hh via 2L-IHP algorithm

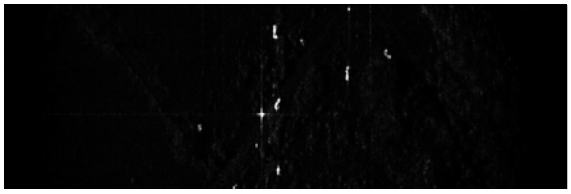

Figure 10: Coherence image of m78p1f23hh via 2L-IHP algorithm

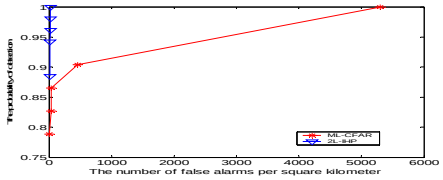

Figure 11: Probability of detection vs. false alarm rate of ML-CFAR and 2L-IHP

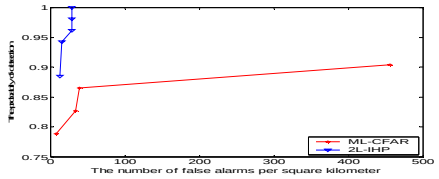

Figure 12: Enlarged view of the low false alarm portion of Figure 11

4. ADJUSTMENT AND IMPROVEMENT OF 2L-IHP ALGORITHM

4.1 Amplitude 2L-IHP

2L-IHP algorithm requires SLC SAR data, which are not easy to get for ordinary users. Amplitude images are the common data we can get. Because the coherence magnitude can be estimated from two multi-look intensity images, and the value is independent of the number of looks (Lee et al., 1994), we consider applying 2L-IHP algorithm in the multi-look amplitude SAR imagery. The Preprocessing like removing the weight function can not be applied here, but the rest resembles 2L-IHP. Figure 13 shows the coherence images coming from 2L-IHP and amplitude 2L-IHP respectively. The original SAR image is extracted from ADTS dataset. It is 100×100 pixels, with an APC in the image center. Though the coherence magnitude from amplitude 2L-IHP is slightly smaller than that from 2L-IHP, the contrast between the target and the clutter is enough for detection.

In order to compare the detection results between the two algorithms, we apply them in the whole ADTS dataset respectively. The dataset contains 52 man-made targets, including military targets and corner reflectors. Table I shows the detection number and false alarm number of the two algorithms. For amplitude 2L-IHP algorithm, all targets

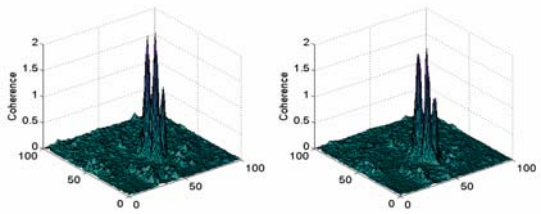

Figure 13: Coherence of 2L-IHP (left) and amplitude 2L-IHP (right)

are detected except one, and the false alarm number is on the same level as the 2L-IHP algorithm. The signal of the lost target is also faint in the 2L-IHP coherence image, which is enhanced only through removing weighting functions. Therefore, we think amplitude data can achieve the same performance as the SLC data in most situations.

Table I: Detecting results of 2L-IHP and amplitude 2L-IHP algorithms for ADTS dataset

Algorithm	total targets	detected targets	false alarms	lost targets
2L-IHP	52	52	11	0
Amplitude 2L-IHP	52	51	10	1

4.2 Polarimetric 2L-IHP

Polarimetric SAR images contain more useful information for target detection than any single channel. A Pol2L-IHP algorithm is also introduced in (Souyris et al., 2003), but SLC data is necessary, too. Many polarimetric SAR images are stored in compressed Stokes matrix. How to get the final detecting image from the four channels is the key of the problem. Among the various methods, PWF (Polarimetric Whitening Filter) (Novak and Burl, 1990 and 1993) gets broad application, which needs to estimate the polarimetric covariance matrix of the clutter. We can acquire the detecting image through PWF before amplitude 2L-IHP algorithm.

4.3 Influence of Different Bands and Polarizations on Target Detection

Different imaging bands affect the detecting result significantly, so do the polarizations. Hence it is necessary to select band and polarization to gain the best result. For this purpose, we apply C-、L- and P band of polarimetric AIRSAR data in our experiments. The AIRSAR data was collected in Tai-chung Taiwan, China,

by NASA/JPL in November 30, 1996. The chirp bandwidth is 40MHz, and the sampling spacing is about 9m (azimuth)×3m (slant range). The number of looks processed in azimuth and range is 18 and 1, respectively. Our experiment area is 500×600 pixels, containing 14 man-made point targets on the top right corner (Figure 14). These targets are adjacent to each other. Due to the influence of the near targets to the mean and variance of the clutter, the traditional CFAR methods can not work here. The data is multi-looked and compressed in Stokes matrix, and amplitude 2L-IHP is applied here.

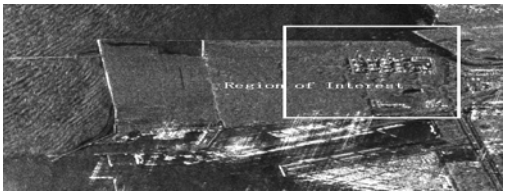

Figure.14: AIRSAR image (C-HH)

4.3.1 Analysis for Single Channel SAR Images

In order to analyze the impact of data to the detecting results, different bands and polarizations AIRSAR images are processed by amplitude 2L-IHP. The results are displayed in Table II (see chapter 4.3.3). The HV channel is not considered here for its bad detecting result. From the table, we can see that C-HH、L-HH and L-VV are on the same detecting level and they perform better than C-VV、P-HH and P-VV. Then how to rank C-HH、L-HH and L-VV? To resolve this question, a quantitative criterion is required. The detection is related directly to the coherence, so the maximum coherence is used to evaluate the detection effect in the images of different bands and polarizations. Larger coherence means better detecting result. Figure 15 shows the coherence of 14 targets in various conditions. C-HH and L-HH have similar coherence values, and the coherence of L-VV is a little lower. Generally speaking, the following conclusions can be drawn about the detecting ability: (1) For the same band, HH > VV > HV (rank decreasingly), and HH is the first choice for target detection; (2) For the same polarization, L > C > P. It is hard to discriminate between C-HH and L-HH, but L band is preferable considering penetrating ability. (3) As a whole, L-HH > C-HH > L-VV. These rules can be referred when we select data source for man-made target detection.

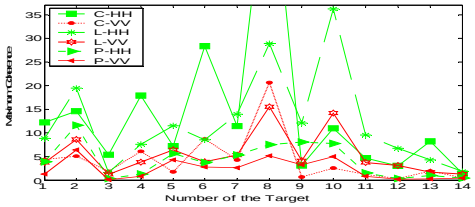

Figure 15: Coherence of 14 man-made targets in HH/VV SAR images

4.3.2 Analysis for Polarimetric SAR Images

It is required to compute the polarimetric covariance matrix of the clutter when PWF is applied. The polarimetric covariance matrix is estimated from a 100×100 pixel clutter area. Amplitude 2L-IHP is processed in the synthetical image. Similarly, the maximum coherences of the targets are used to compare the detecting ability of different bands (Figure 16). Analogical to the single channel, L- and C band are better than P band, but the relationship between the two is difficult to determine without considering other factors.

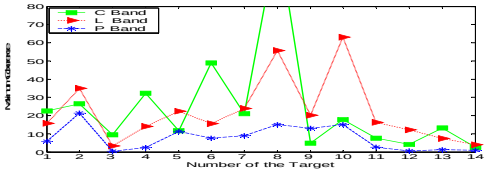

Figure 16: Coherence of 14 man-made targets in polarimetric SAR images

4.3.3 Comparison between Single Channel and Polarimetric Imagery

The coherence magnitude of man-made target in the polarimetric SAR image is larger than that in the single channel. The former is about 1.8 times the latter in C band (Figure 17). It is similar to L- and P band. However, for P band the coherence is much lower than the normal threshold, so the target is likely lost in the detecting process. In 2L-IHP algorithm, large coherence means easy to detect, therefore polarimetric image is better than the corresponding single channel. The relationship of the two can be viewed in another perspective, that is, from the number of the final detected targets. The detecting results of different bands are shown in Table II. However, it can not be inferred only from the Table II that polarimetric images perform better than the single channel. Of course, the polarimetric images always produce the best probability of target detection, compared to the single channel of the same band.

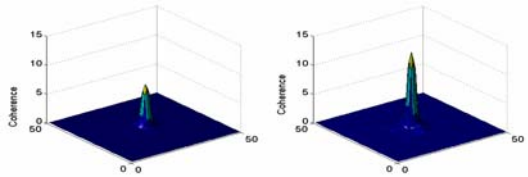

Figure 17: Coherence of C-band HH (left) and polarimetric (right) SAR images

Table II: detecting results of sar images from different bands and polarizations

Band	C-HH	C-VV	C-Pol	L-HH	L-VV	L-Pol	P-HH	P-VV	P-Pol
Detected Targets	14	11	14	14	14	14	12	11	12
Lost Targets	0	3	0	0	0	0	2	3	2

5. CONCLUSION

In this paper two kinds of detecting algorithms, CFAR and 2L-IHP, are briefly introduced and compared first. Exploiting the ADTS data set, we demonstrate that 2L-IHP not only detect all the man-made targets but also produce lower probability of false alarm than ML-CFAR. Then amplitude 2L-IHP and polarimetric 2L-IHP are generated to circumvent the data constraint. Though the coherence is slightly lower than that from 2L-IHP, it still can discriminate between the man-made target and the clutter. What's important is that it is effective for amplitude images. From the experiments implemented in the AIRSAR data, we draw some useful conclusions about the detecting ability: (1) For the same polarization, HH > VV > HV; (2) For the same polarization but different band, L > C > P (considering the penetrating ability of the band); (3) For all single channels, C-HH and L-HH achieve the best results; (4) Considering from the perspective of coherence, the polarimetric image performs better than the single channel image. Due to the lack of sufficient data, these conclusions need validating further.

REFERENCES

1. Burl M. C., G. J. Owirka, and L. M Novak (1989). Texture Discrimination in Synthetic Aperture Radar Imagery. 23rd Asilomar Conf. on Signals, Systems, and Computers, Pacific Grove, CA, pp. 399-404.
2. Famil L. F., A. Reigber, E. Pottier and W. M. Boerner (2002). Scene Characterization Using Sub-Aperture Polarimetric SAR data Analysis. Proceedings of IGARSS '02, Toronto, Canada, pp. 417-419.
3. Koch M. W. and M. M. Moya (1995). Cueing Feature Discovery and one-class Learning for Synthetic Aperture Radar Automatic Target Recognition. Neural Networks, 8(7/8): 1081-1102.
4. Kuttikkad S. and R. Chellappa (1994). Non-Gaussian CFAR Techniques for Target Detection in High Resolution SAR Images. In: Proceedings of IEEE International Conference On Image Processing, Austin, Texas, USA, pp. 910-914.
5. Lee J. S., K. W. Hoppel, S. A. Mango, and A. R. Miller (1994). Intensity and Phase Statistics of Multilook Polarimetric and Interferometric SAR Imagery. IEEE Transactions on Geoscience and Remote Sensing, 32(5): 1017-1028.
6. McConnell I. and C. J. Oliver (1998). A Comparison of Segmentation Methods with Standard CFAR for Point Target Detection. In: Europto Conf. on SAR Image Analysis, Simulation and modeling IV, Orlando, FL, USA, SPIE 3497: 76-87.
7. McConnell I. and C. J. Oliver (1999). Segmentation-based Target Detection in SAR. In: Europe Conf. on SAR Image Analysis, Modelling and Techniques II, Florence, Italy, SPIE 3869: 45-54.
8. Meth R. (2002). Synthetic Aperture Radar Vehicle Detection via Subaperture Coherence. http://www.asc2002.com/anuscripts/J/Jo-02.PDF.
9. Novak L. M.and M. C. Burl (1993). Optimal Polarimetric Progressing for Enhanced Target Detection. IEEE Transactions on Aerospace and Electronic System, 29(1): 234-244.
10. Novak L. M.and M. C. Burl (1990). Optimal Speckle Reduction in Polarimetric SAR Imagery . IEEE Transactions on Aerospace and Electronic System, 26(2): 293-305.
11. Principe J. C. and A. Radisavljevic (1998). Target Prescreening Based on a Quadratic Gamma Discriminator. IEEE Transactions on Aerospace and Electronic Systems, 34(3): 706-715.
12. Ravid R. and N. Levanon (1992). Maximum-likelihood CFAR for Weibull Background. Radar and Signal Processing, IEE Proceedings-F, 139(3): 256-264.
13. Souyris J. C., C. Henry and F. Adragna (2003). On the Use of Complex SAR Image Spectral Analysis for Target Detection: Assessment of Polarimetry. IEEE Transactions on Geoscience and Remote Sensing, 41(12): 2725-2734.
14. Henry C., J. C. Souyris and P. Marthon (2003). Target Detection and Analysis Based on Spectral Analysis of a SAR Image: a Simulation Approach. Proceedings of IGARSS '03, Toulouse, France, pp. 2005-2007.